Automated detection of exudates for diabetic retinopathy screening

2007 Phys. Med. Biol. 52 7385

(http://iopscience.iop.org/0031-9155/52/24/012)

IOP Publishing Physics in Medicine and Biology

Phys. Med. Biol. **52** (2007) 7385–7396 doi:10.1088/0031-9155/52/24/012

Automated detection of exudates for diabetic retinopathy screening

Alan D Fleming[1], Sam Philip[2], Keith A Goatman[1], Graeme J Williams[2], John A Olson[2] and Peter F Sharp[1]

[1] Biomedical Physics, University of Aberdeen, Aberdeen, AB25 2ZD, UK
[2] Diabetes Retinal Screening Service, David Anderson Building, Foresterhill Road, Aberdeen, AB25 2ZP, UK

E-mail: a.fleming@abdn.ac.uk

Received 7 August 2007, in final form 15 November 2007
Published 5 December 2007
Online at stacks.iop.org/PMB/52/7385

Abstract

Automated image analysis is being widely sought to reduce the workload required for grading images resulting from diabetic retinopathy screening programmes. The recognition of exudates in retinal images is an important goal for automated analysis since these are one of the indicators that the disease has progressed to a stage requiring referral to an ophthalmologist. Candidate exudates were detected using a multi-scale morphological process. Based on local properties, the likelihoods of a candidate being a member of classes exudate, drusen or background were determined. This leads to a likelihood of the image containing exudates which can be thresholded to create a binary decision. Compared to a clinical reference standard, images containing exudates were detected with sensitivity 95.0% and specificity 84.6% in a test set of 13 219 images of which 300 contained exudates. Depending on requirements, this method could form part of an automated system to detect images showing either any diabetic retinopathy or referable diabetic retinopathy.

1. Introduction

Screening for diabetic retinopathy is widely recognized as a cost-effective means for reducing the incidence of blindness in people with diabetes (James *et al* 2000, Sculpher *et al* 1992). The currently recommended examination technique for diabetic retinal screening in the UK is digital fundus photography (Facey *et al* 2002, Garvican *et al* 2000, Olson *et al* 2003). It is widely accepted that computer automation of image grading would allow the grading workload and associated costs to be reduced and may be more reliable than the existing manual grading (Screening for Diabetic Retinopathy in Europe 2006, Usher *et al* 2004, Philip *et al* 2007).

Diabetic retinopathy occurs as a result of vascular changes in the retina causing swellings of capillaries, known as microaneurysms (MA). These may eventually become a source of leakage of plasma causing thickening of the retina, or oedema, and, if occurring in the macular region, can cause loss of high quality vision. Unfortunately, retinal thickening is not easily visible in fundus photographs and hence associated fat deposits, known as exudates, are used as a surrogate marker. Being highly reflective these are easily visible in retinal photographs. Exudates commonly form clusters, and may be distributed across the retina or may appear in a ring around a central point of leakage. Although most exudates appear as small dots or irregular patches, the directional nature of the nerve fibre layer may cause individual exudates to have a linear shape. The presence of exudates has high sensitivity, though low specificity, as an indicator of macular oedema; patients presenting with exudates in the macular region are normally referred to an ophthalmology clinic where slit-lamp biomicroscopy can confirm the presence or absence of macular oedema.

This paper describes an automated method for detecting exudates in images obtained during diabetic retinopathy screening. To attain high agreement with human expert identification, it is necessary to detect very small isolated exudates and this task is made more difficult by the presence of two other types of retinal pathology which produce bright objects. Firstly, there are drusen that usually appear in clusters, with a characteristic 'pebbled' appearance. They are more orange, less yellow, than exudates and appear less sharply defined. Drusen are not a sign of diabetic retinopathy but are linked to age-related macular degeneration. Secondly, there are cotton wool spots, which are more fuzzy and are usually larger than exudates and tend to be isolated. Other bright areas in retinal images are caused by specular reflections mainly originating from the internal limiting membrane (ILM) in younger patients and from abnormalities of the vitreous. Circular scars resulting from pan-retinal photocoagulation (PRP) treatment for diabetic retinopathy are also highly reflective.

Reported performances of prior work on exudate detection are shown in table 1. Most have not explicitly handled drusen, cotton wool spots or specular reflections though a notable exception is (Niemeijer *et al* 2007). This describes a system trained to identify bright lesions and to classify them as exudates, drusen or cotton wool spots, achieving a sensitivity and specificity of 95% and 86%, respectively, for detection of images containing exudates. At most 54 images with exudates have been used to test exudate detection in the studies listed in table 1.

2. Material

Images used in this study were drawn from 14 406 anonymized images from 6722 patients attending the Grampian Diabetes Retinal Screening Programme in North-East Scotland during 2003–2004. Our image quality analysis (Fleming *et al* 2006a), based on the visibility of the macular vessels, excluded 853 images as being unsuitable for retinopathy analysis. The training sets and the test set were drawn from the remaining 13 553 images. The images contained 2160 $\times$ 1440 pixels and were obtained with non-mydriatic photography using 45° Canon CR5-45NM and CR6-45NM fundus cameras attached to Canon D30 digital colour cameras.

All images had been graded by a clinical research fellow for all signs of diabetic retinopathy as well as drusen, cotton wool spots, ILM reflections and PRP scars. Exudates were graded according to whether they were $\leqslant 2$ but >1 optic disc diameters (DD) from the fovea, a sign of observable retinopathy, requiring the patient to be screened at a reduced interval, or $\leqslant 1$ DD from the fovea, a sign of referable retinopathy, requiring referral to an ophthalmologist (Facey *et al* 2002). According to the clinical research fellow grading, the

Table 1. Reported exudate detection results.

Reference	Sensitivity	Specificity	Test set
Task: to detect images with exudates			
Hsu *et al* (2001)	100%	74.2%	543 images (31 with exudates, drusen present)
Lee *et al* (2001)	96%	93%	422 images (54 with exudates)
Li and Chutatape (2004)	100%	71%	35 images (28 with exudates)
Niemeijer *et al* (2007)	95%	86%	300 images (42 with exudates, 52 with drusen, 30 with cotton wool spots)
Osareh *et al* (2003)	93.0%	94.1%	67 images (27 with exudates)
Wang *et al* (2000)	100%	70%	154 images (54 with exudates)
Task: to detect image segments with exudates			
Gardner *et al* (1996)	93.1%	93.1%	2000 segments with 20× 20 pixels (1000 segments with exudates)
Sinthanayothin *et al* (2002)	88.5%	99.7%	60790 segments with 10× 10 pixels (from 30 images, 21 with exudates)
Task: to detect pixels belonging to exudates			
Phillips *et al* (1993)	87%	98.5%[a]	Pixels in 30 regions of 13 images
Walter *et al* (2002)	92.8%	92.4%[a]	Pixels in 15 images
Task: to distinguish exudates from cotton wool spots			
Ege *et al* (2000)	98.9%	80%	170 exudates and 25 cotton wool spots

[a] Predictive value.

prevalence of exudates in the 14 406 images was 2.9% (412) of which exudates $\leqslant 2$ and >1 DD from the fovea had a prevalence of 2.3% (326) and exudates $\leqslant 1$ DD from the fovea had a prevalence of 1.9% (272). The prevalences of other bright features were drusen 6.7% (967), cotton wool spots 0.5% (65), ILM reflections 6.0% (861) and PRP scars 0.7% (107).

3. Methods

Candidate exudates were located using multi-scale morphology. These were classified based on locally evaluated features to generate a likelihood that each candidate is exudate, drusen or background. Classifications of images, as containing exudates or not, were generated by combining the likelihoods calculated for each candidate.

3.1. Pre-processing

The green plane of the colour image was filtered to reduce noise, first with a 3× 3 median filter and then by convolution with a Gaussian filter, $\sigma = 2$. The background intensity, denoted as K, was estimated by applying a 121× 121 median filter. A shade-corrected image was generated with

$$J' = I/K - 1 \tag{1}$$

and was normalized for global image contrast by dividing by its standard deviation (sd):

$$J = J'/\mathrm{sd}(J'). \tag{2}$$

The value of J at an exudate was typically +6 to +1.5 while retina was typically −0.5 to +0.5 and dark features such as vessels were typically −6 to −1.5. Since the highly reflective optic disc could be falsely identified as exudate, it is located automatically as described in (Fleming *et al* 2007). A circular region of diameter 306 pixels, centred on the detected optic

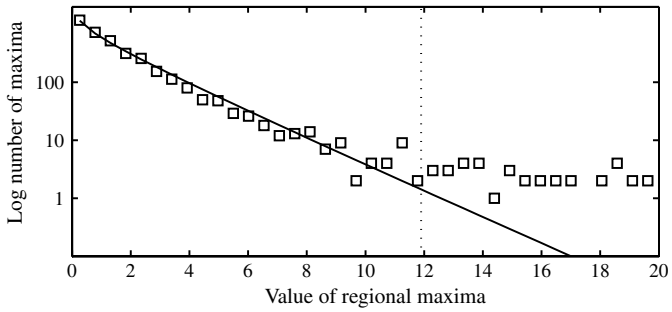

Figure 1. Log number of regional maxima in $D^{(1)}$ against the values of the maxima (squares) for a sample retinal image and the fitted gamma distribution (solid line). Threshold $t^{(1)}$ is indicated by a dotted line.

disc centre, is excluded from further analysis. This is about 30% larger than the average optic disc diameter so that anomalous regions of retina close to the disc are also excluded.

3.2. Candidate detection

We have shown in earlier work (Fleming *et al* 2006b, Hipwell *et al* 2000, Cree *et al* 1997) that the difference between an image and the minimum of its closings by multiple linear structuring elements highlights dark dots, such as MAs, while suppressing linear vascular structures. Linear bright structures are not so obvious in retinal images but do occur particularly where the nerve fibre layer is prominent and where there is increased reflectance of the retina adjacent to vessels. Therefore, an inversion of the technique used to detect MA candidates is also suitable for detection of exudate candidates. Initial tests showed that the use of multiple linear structuring elements out-performs opening by a single disc shaped structuring element for exudate detection. The difference between the original image and the maximum of openings by multiple linear structuring elements was performed at five scales:

$$D^{(s)} = J^{(s)} - \max_{n=0\ldots7} (J^{(s)} \circ \lambda(p, n\pi/8)), \tag{3}$$

where $J^{(s)}$ are under-sampled versions of J by a factor of 2^{s-1} after application of an anti-aliasing filter, $s = 1, \ldots, 5$, '$\circ$' represents morphological greyscale opening, $\lambda(p, \alpha)$ represents a linear structuring element containing $p = 11$ pixels approximating a line at angle α. The result, $D^{(s)}$, is an enhancement of bright dots present in the original image at scale s.

Due to the presence of other bright features in retinal images and due to natural variations in retinal reflectivity, most of the dots in $D^{(s)}$ are not exudates. Dynamic thresholding was performed by using maximum likelihood estimation to fit a gamma distribution, as in figure 1, to the set, $M^{(s)}$, of intensities of regional maxima of each $D^{(s)}$. A threshold, $t^{(s)}$, was determined where the cumulative fitted gamma distribution is $1 - \frac{N_{FP}}{\text{card}(M^{(s)})}$ with $\text{card}(M^{(s)})$ being the number of data samples in $M^{(s)}$ and with $N_{FP} = 5$ being an estimate of the number of false positive candidates that can be tolerated in an image at each scale. Exudate candidates were taken at the regional maxima in J within regions for which, at some scale, $D^{(s)}$ is greater than $t^{(s)}$.

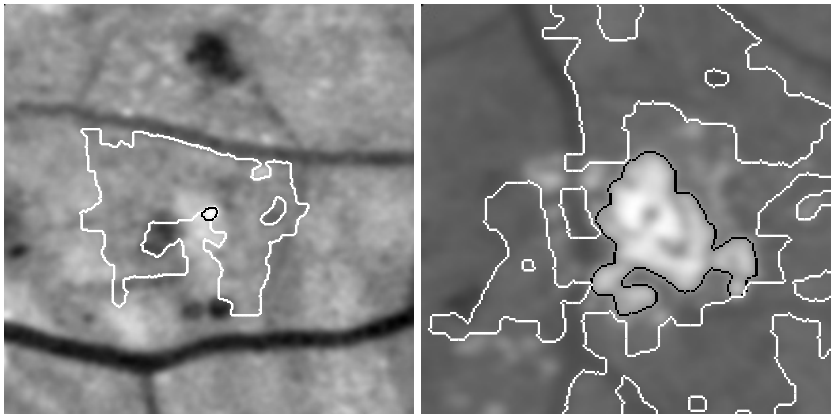

Figure 2. Examples of region growing around exudate candidates. Region growing result, R, is indicated by a black line and the result of watershed retinal region growing, B, by a white line.

3.3. Candidate evaluation

Region growing is performed around each candidate by applying a reducing threshold until the mean gradient magnitude along the region border is maximized as in (Fleming *et al* 2006b). The resulting region is denoted by R. Examples are shown in figure 2.

Further region growing is performed as described in the watershed retinal region growing section in (Fleming *et al* 2006b). This region growing technique finds a region of retina that avoids vessels and other lesions. The watershed transform is applied to the gradient magnitude image of J. Watershed regions are each given an intensity which is the mean of J over the region. Watershed regions are merged one at a time starting with the region adjacent to R whose intensity is closest to zero. Subsequent regions are chosen so as to minimize the difference between the intensity of the added region and the mean of intensities of the previously merged watershed regions. Region growing is stopped if the region size becomes larger than a threshold or if the intensity of the added region is much different (more than two standard deviations away from the mean) from the intensities of the previously merged watershed regions. The result of this region growing is denoted by B, figure 2. It does not intersect R.

The region B is used for evaluating mean luminosity, $L_{\mathrm{bg}} = \mathrm{mean}(J(B))$, and contrast, C_{bg}, in the local background to a candidate. Contrast is the standard deviation within B of J high-pass filtered, taking into account the boundary of B:

$$J^B_{\mathrm{hpf}} = \left[J - \frac{(J \times B) * G(16)}{B * G(16)} \right] \tag{4}$$

$$C_{\mathrm{bg}} = \mathrm{sd}\left(J^B_{\mathrm{hpf}}(B)\right), \tag{5}$$

where B is treated as a numerical image, valued 1 within the region and zero outside, '$\times$' represents pixelwise multiplication, '$*$' represents convolution and $G(\sigma)$ represents a two-dimensional Gaussian kernel with variance σ^2.

3.4. Classification of candidates

Since drusen are a common distraction for exudate detection, images with drusen were deliberately included during training. A set of 96 images (28 with exudates only, 30 with

Table 2. Features evaluated at each exudate candidate.

Feature	Description
1	The normalized luminosity, $(\text{mean}(J(R)) - L_{\text{bg}})/C_{\text{bg}}$
2	The normalized standard deviation (sd) of luminosity, $\text{sd}(J(R))/C_{\text{bg}}$
3	The normalized boundary gradient calculated as the mean gradient magnitude of J along the boundary of R divided by C_{bg}
4	The candidate area, A, evaluated as the number of pixels in R
5	The spread of R evaluated as $(\sqrt{A}/\bar{d} - 3\sqrt{\pi})/2$, where $\bar{d}$ is the mean distance of pixels in R from its boundary. This has a minimum of 0 for a circle
6	The distance of the candidate from the nearest MA detected as in (Fleming *et al* 2006b)
7, 8	Standardized colour features. A good quality well-exposed retinal image was chosen as a standard. Histogram standardized image planes were generated by applying a strictly increasing transformation to the red and green colour planes of I so that each result had a histogram which is similar to that of the corresponding plane of the standard image. The mean was taken of the standardized red and green planes over R

drusen only) was used for training the classification of candidates. The locations of exudate candidates were determined in the manner described above. The 28 images with exudates were displayed sequentially with the locations of candidates overlayed. Candidates in these images judged not to be exudates were rejected, leaving 280 candidates that were classed as exudates. For the 30 images with drusen, all candidates that were judged not to be drusen were rejected, leaving 238 candidates that were classed as drusen. All 490 candidates generated from the remaining 38 images that contained neither exudates nor drusen were classified as background.

The features listed in table 2 were evaluated at each candidate and include size, brightness, area, shape, colour and contextual information, the latter being the distance from the nearest MA. All features were normalized by dividing each by the standard deviation of the feature's values in the training set candidates. A support vector machine (SVM) classifier (Chang and Lin 2001), having radial basis function kernel and trained with normalized features from the training set, was used to classify test candidates as exudate, drusen or background. Since the basic SVM performs binary classification, each of the classes was compared to each of the others in three one-against-one applications of the SVM and the mean was taken of the results. The outputs of the SVM were treated as likelihoods, summing to 1, that each test candidate is a member of each of the classes exudate, drusen or background.

A further training set of 379 images (139 with exudates, 120 with drusen) was used to determine the optimal method for classification of individual candidates and for the detection of images with exudates. The set of features listed in table 2 was found to be optimal compared to sets containing other features (for example using the blue colour plane or replacing features 1, 2 and 3 in the table with versions not normalized by L_{bg} and C_{bg}). It was found that summing the two greatest likelihoods of candidates being exudates (as output from the SVM for each candidate) $\leqslant 2$ DD from the fovea gave the optimum detection of images with exudates,

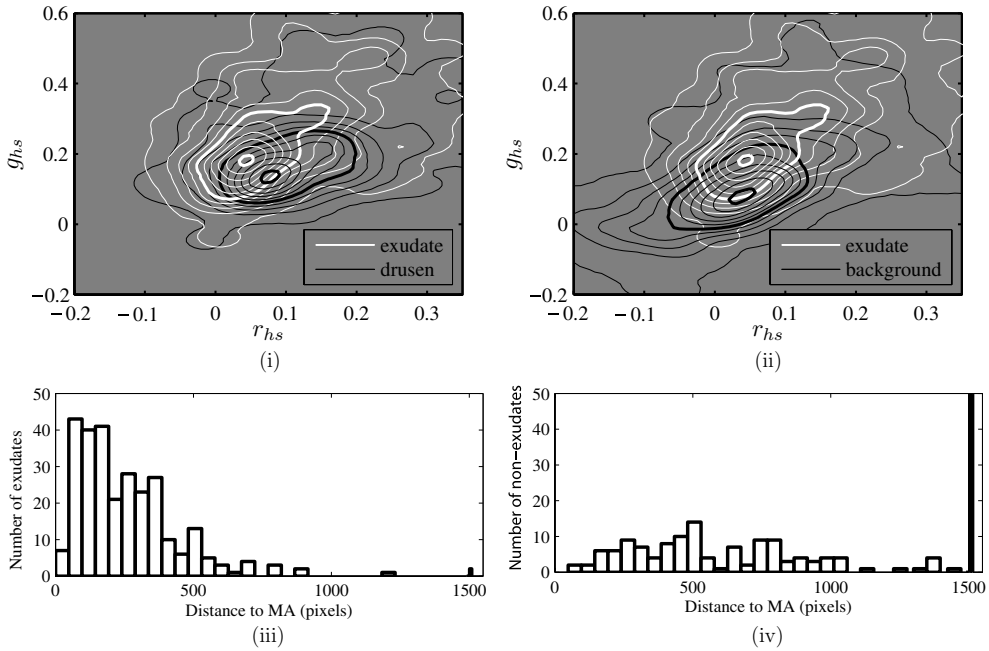

Figure 3. Comparison of the distributions of colour and contextual features for exudates and non-exudates for candidates in the training set. Contour plots illustrate density of candidates when plotted on axes representing standardized red and green intensities for exudates and drusen (i) and for exudates and background (ii). Middle and highest contours are in bold. The histograms show distributions of distances for true exudates (iii) and drusen and background (iv). The bar in (iii) and (iv) at 1500 (greater than image width) represents the number of candidates occurring in images without MAs and extends to 602 in (iv).

assessed by the area under a receiver operator characteristics (ROC) curve. The fovea position was determined as in (Fleming *et al* 2007).

Similarly, it was found that summing the five greatest likelihoods of candidates being drusen $\leqslant$2 DD from the fovea gave the optimum detection of images containing drusen.

4. Results

Figure 3 illustrates the distribution of the colour and contextual features (distance to nearest MA) for candidates in the training set used for classification of candidates. Parts (i) and (ii) use contour plots to illustrate the density of candidates plotted against their standardized red and green features as described in table 2. The figure shows that the true exudates, drusen and background can be partly distinguished by colour. Parts (iii) and (iv) show histograms of distances of candidates from MAs illustrating that true exudates are predominantly close to a MA compared to drusen and background.

After removing the training sets from the images available for the study, a test set of 13 219 images remained with clinical research fellow classifications as follows: 300 with exudates $\leqslant$2 DD from the fovea, of which 199 had exudates $\leqslant$1 DD from the fovea, 842 with drusen, 64 with cotton-wool spots, 857 with ILM reflections and 100 with PRP scars. 13.4% (1825) of

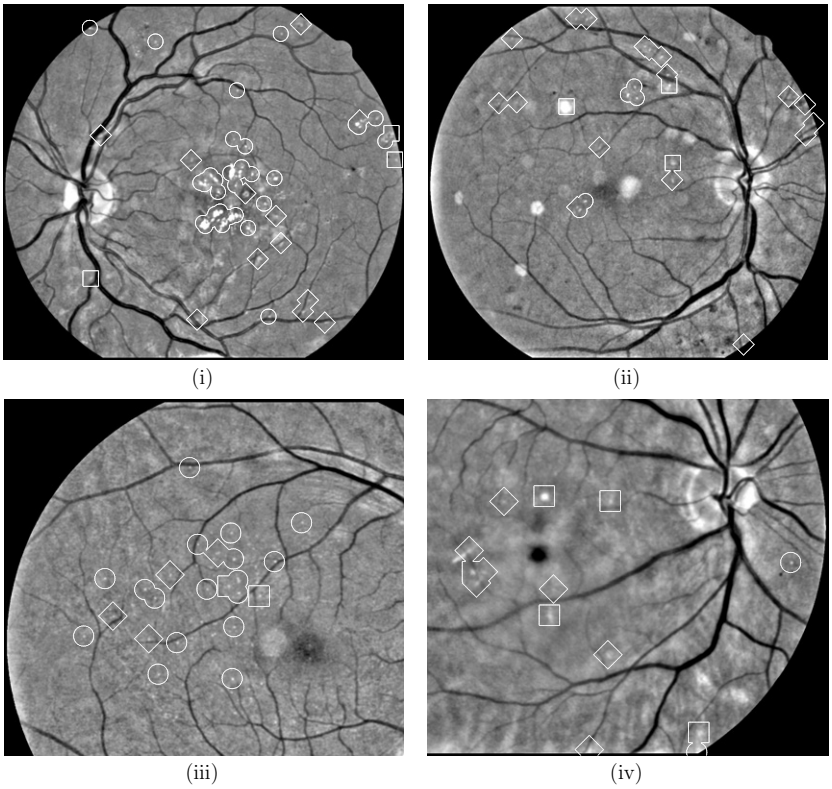

Figure 4. Example results illustrating candidates according to the classification with highest likelihood; circle = exudate, diamond = drusen, square = background. Images were chosen randomly from categories as follows: (i) and (ii) from true positives, (iii) from false positives and (iv) from false negatives.

the images without exudates contained one of the other categories of bright objects. Figure 4 shows examples of image processing results including two images which were true positive results, one which was a false positive result and one which was a false negative result.

Figure 5 shows ROC curves for exudate detection $\leqslant$2 DD and $\leqslant$1 DD from the fovea in the full set of test images and for the subset in which MAs were detected. Areas under the curves, Az, and 95% confidence intervals were calculated using SPSS release 15.0.0 (SPSS Inc., Illinois). Results were obtained and plotted with and without using contextual information, the distance to the nearest MA. Az shows a significant increase, for tests using all images, by adding contextual information for exudates $\leqslant$2 DD and $\leqslant$1 DD from the fovea (both cases $p < 0.0001$ determined by ROCKIT software, Kurt Rossman Laboratories). A ROC curve for detection of images with drusen is shown.

Table 3 shows a cross-tabulation of the image classifications made by the clinical research fellow against automated image classifications. Column categories are the clinical research fellow indications exudate, drusen, cotton-wool spots, ILM reflections, PRP scars and none. Images with more than one of these features were assigned to the leftmost of the relevant categories; for example, images containing exudates and another category of bright objects were entered in the 'Exudates' column. The rows indicate the automated system classification of images as containing exudates, drusen or none. These classifications were obtained by

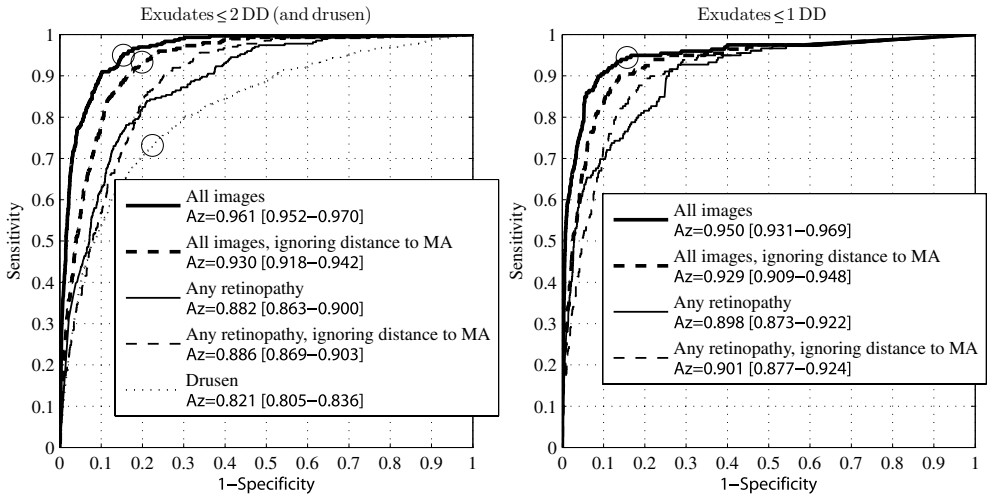

Figure 5. Receiver operator characteristics curves for automated detection of images with exudates ⩽2 DD and ⩽1 DD from the fovea. For the dashed curves, classification was made without contextual information, the distance to the nearest MA. Thick lines are for the full test set and fine lines are for images in which MAs were detected ('any retinopathy'). Circles indicate operating points; those in the left-hand plot were used to generate table 3. Areas under the curves, Az, are given with 95% confidence intervals (square brackets). The dotted curve in the left-hand plot is for the detection of images containing drusen.

Table 3. Cross tabulation of bright objects observed by the clinician and by automated image classifications.

	Clinician:	None	Exudates[a]	Drusen	Cotton wool spots	ILM reflections	PRP scars	Total
				Using contextual information				
Auto-	None	8153	4	160	18	208	8	8551
mated:	Exudates	1261	285	205	26	435	60	2272
	Drusen	1740	11	458	9	174	4	2396
				Not using contextual information				
	None	7946	5	129	30	179	11	8300
	Exudates	1556	280	373	12	594	36	2851
	Drusen	1652	15	321	11	44	25	2068
	Total	11 154	300	823	53	817	72	13 219

[a] ⩽2 DD from the fovea.

imposing thresholds that achieve equal sensitivity and specificity for exudates and equal sensitivity and specificity for drusen in the training set and correspond to the operating points shown by circles in figure 5.

5. Discussion

This paper has assessed the ability of an automated exudate detection system, based on classification of individual bright objects, using images drawn from a diabetic retinal screening programme. Images with referable or observable exudates (⩽2 DD from the fovea) were

recognized at sensitivity 95.0% and specificity 84.6% and images with referable exudates ($\leqslant$1 DD from the fovea) were recognized at sensitivity 94.5% and specificity 84.3%. A large proportion of false positive detections were images containing ILM reflections. However, most false positive detections occur in images in which no bright objects had been recorded by the clinician.

The test set, with exudates present in 300 images, is larger than any previously reported study. A multi-scale and dynamic thresholding method has been used to detect candidates. As with several other studies (Niemeijer *et al* 2007, Ege *et al* 2000, Osareh *et al* 2003, Wang *et al* 2000), each potential lesion is classified according to local features such as colour, brightness, sharpness, area and others. We have used a three-way classification that includes drusen, the most prevalent bright lesion in the screened population. In addition, we have made use of two other techniques. Firstly, local contrast normalization was used to compare brightness of an object to the contrast in its local background and secondly, contextual information in the form of the distance to the nearest MA was used. The presence of dark lesions was also used in (Niemeijer *et al* 2007) to assist exudate detection but the advantage of doing so was not analysed. Contextual information of a different nature was used in (Hsu *et al* 2001) where a significant improvement was attained by excluding bright objects in the proximity of vessels. Given our large test set of unselected images our results compare favourably with previous studies.

Figures 3 (iii) and (iv) show that exudates are much more likely to be present in images with MAs than in images without MAs. Hence, as shown by the bold solid and dashed lines in figure 5, the presence of MAs assists detection of images with exudates, significantly increasing the area under the ROC curve from $Az = 0.930$ to $Az = 0.961$ ($\leqslant$2 DD) and $Az = 0.929$ to $Az = 0.950$ ($\leqslant$1 DD). Figures 3 (iii) and (iv) also show that there is a tendency for exudates to be closer to a detected MA than drusen or background candidates. Despite this, the areas under the fine solid and dashed curves of figure 5 show that this information does not improve exudate detection when applied only to images containing MAs. This may be due to the low sensitivity for individual MA detection compared to detection of images with MAs (Fleming *et al* 2006b) so that the presence of any MA in an image is a more robust measure than the distance to an individual MA.

Although it is necessary to check the performance of automated systems by comparison with a human observer, it should be recognized that opinions concerning the disease content of retinal images can differ substantially (Ruamviboonsuk *et al* 2006). In studies comparing automated exudate detection (table 1) with human expert detection, a retinal specialist attained 90% sensitivity and 98% specificity compared to a reference standard (Niemeijer *et al* 2007) and a retinal specialist attained 53% sensitivity and 99% specificity compared to a general ophthalmologist (Lee *et al* 2001). The latter of these results is close to the ROC curve in figure 5 (left).

Exudate detection could be used to augment an automated system for screening of diabetic retinopathy such as the one we have described in (Philip *et al* 2007). This system detects patients with any diabetic retinopathy who comprise roughly 30% of the total and those with photographs of inadequate quality. The system uses MA detection since these lesions are the earliest sign of diabetic retinopathy and are present throughout the course of the disease. Five out of 330 cases of referable retinopathy were missed by this system and all contained exudates. Therefore, exudate detection may increase the likelihood of detection of the few cases of referable retinopathy in which an automated system does not detect MAs.

An alternative scenario for automated grading would be to detect only patients with referable retinopathy. Clinically this may be regarded as a satisfactory outcome since patients with earlier forms of the disease are not treated (Facey *et al* 2002). For this to be successful,

exudate detection would need to be combined with the detection of other signs of referable retinopathy including haemorrhages and possibly new vessel growth.

The system could also be used to check the presence of drusen though the accuracy is poorer than for exudates. Given that (Niemeijer *et al* 2007) also found that exudates could be more easily detected than drusen; this probably reflects the intrinsic relative difficulties of the tasks.

This paper has described a system which could play a part in detecting images with any diabetic retinopathy or with referable retinopathy. Most images with drusen are discarded though other types of bright features are likely to cause false positive recognitions. The relatively high prevalence of specular reflections suggests that a system with the ability to distinguish lesions from these artefacts would be a goal worthy of future investigation. Other automated tasks must be combined with those described here to form a fully automated diabetic retinopathy detection system and further work is required to evaluate the combined performance. The success of the exudate detection method described here suggests that undertaking such an evaluation would be worthwhile.

References

Chang C C and Lin C J 2001 LIBSVM: a library for support vector machines. Software available at http://www.csie.ntu.edu.tw/~cjlin/libsvm

Cree M J, Olson J A, McHardy K C, Sharp P F and Forrester J V 1997 A fully automated comparative microaneurysm digital detection system *Eye* **11** 622–8

Ege B M, Hejlesen O K, Larsen O V, Moller K, Jennings B, Kerr D and Cavan D A 2000 Screening for diabetic retinopathy using computer based image analysis and statistical classification *Comput. Methods Programs Biomed.* **62** 165–75

Facey K, Cummins E, Macpherson K, Morris A, Reay L and Slattery J 2002 Organisation of services for diabetic retinopathy screening *Health Technology Assessment Report* 1 (Technical Report Health Technology Board for Scotland Glasgow)

Fleming A D, Goatman K A, Philip S, Olson J A and Sharp P F 2007 Automatic detection of retinal anatomy to assist diabetic retinopathy screening *Phys. Med. Biol.* **52** 331–45

Fleming A D, Philip S, Goatman K A, Olson J A and Sharp P F 2006a Automated assessment of diabetic retinal image quality based on clarity and field definition *Invest. Ophthalmol. Vis. Sci.* **47** 1120–5

Fleming A D, Philip S, Goatman K A, Olson J A and Sharp P F 2006b Automated microaneurysm detection using local contrast normalization and local vessel detection *IEEE Trans. Med. Imaging* **25** 1223–32

Garvican L, Clowes J and Gillow T 2000 Preservation of sight in diabetes: developing a national risk reduction programme *Diabet. Med.* **17** 627–34

Hipwell J H, Strachan F, Olson J A, McHardy K C, Sharp P F and Forrester J V 2000 Automated detection of microaneurysms in digital red-free photographs: a diabetic retinopathy screening tool *Diabet. Med.* **17** 588–94

Hsu W, Pallawala P M D S, Lee M L and Eong K G A 2001 pp 246–51 The role of domain knowledge in the detection of retinal hard exudates *Proc: IEEE Computer Society Conference on Computer Vision and Pattern Recognition* vol 2 (Kauai, Hawaii)

James M, Turner D A, Broadbent D M, Vora J and Harding S P 2000 Cost effectiveness analysis of screening for sight threatening diabetic eye disease *Br. Med. J.* **320** 1627–31

Lee S C, Lee E T, Kingsley R M, Wang Y M, Russell D, Klein R and Warn A 2001 Comparison of diagnosis of early retinal lesions of diabetic retinopathy between a computer system and human experts *Arch. Ophthalmol.* **119** 509–15

Niemeijer M, Ginneken B v, Russel S R, Suttorp-Schulten M S A and Abramoff M D 2007 Automated detection and differentiation of drusen, exudates and cotton-wool spots in digital color fundus photographs for diabetic retinopathy diagnosis *Invest. Ophthalmol. Vis. Sci.* **48** 2260–7

Olson J A, Strachan F M, Hipwell J H, Goatman K A, McHardy K C, Forrester J V and Sharp P F 2003 A comparative evaluation of digital imaging, retinal photography and optometrist examination in screening for diabetic retinopathy *Diabet. Med.* **20** 528–34

Osareh A, Mirmehdi M, Thomas B and Markham R 2003 Automated identification of diabetic retinal exudates in digital colour images *Br. J. Ophthalmol.* **87** 1220–3

Philip S, Fleming A D, Goatman K A, Fonseca S, Mcnamee P, Scotland G S, Prescott G J, Sharp P F and Olson J A 2007 The efficacy of automated 'disease/no disease' grading for diabetic retinopathy in a systematic screening programme *Br. J. Ophthalmol.* **91** 1512–7

Ruamviboonsuk P, Teerasuwanajak K, Tiensuwan M and Yuttitham K 2006 Interobserver agreement in the interpretation of single-field digital fundus images for diabetic retinopathy screening *Ophthalmology* **113** 826–32

Screening for Diabetic Retinopathy in Europe 2006 *Screening for Diabetic Retinopathy in Europe 15 years after the St. Vincent Declaration* Liverpool, UK, http://www.drscreening2005.org.uk/conference_report.doc

Sculpher M J, Buxton M J, Ferguson B A, Spiegelhalter D J and Kirby A J 1992 Screening for diabetic retinopathy: a relative cost-effectiveness analysis of alternative modalities and strategies *Econ. Health* **1** 39–51

Usher D, Dumskyj M, Himaga M, Williamson T H, Nussey S and Boyce J 2004 Automated detection of diabetic retinopathy in digital retinal images: a tool for diabetic retinopathy screening *Diabet. Med.* **21** 84–90

Wang H, Hsu W, Goh K G and Lee M L 2000 pp 181–6 Effective approach to detect lesions in color retinal images *Proc: IEEE Computer Society Conference on Computer Vision and Pattern Recognition* vol 2 (South Carolina)